Bio-Design and Manufacturing (2023) 6:12–25
https://doi.org/10.1007/s42242-022-00219-x

RESEARCH ARTICLE

Three-dimensional kagome structures in a PCL/HA-based hydrogel scaffold to lead slow BMP-2 release for effective bone regeneration

Se-Hwan Lee[1] · Kang-Gon Lee[2] · Jaeyeon Lee[2] · Yong Sang Cho[3] · Min-Soo Ghim[4] · Soojin Kim[5] · Su-Jin Heo[1] · Yongdoo Park[2] · Young-Sam Cho[6,7] · Bu-Kyu Lee[5,8]

Received: 16 March 2022 / Accepted: 7 October 2022 / Published online: 3 December 2022

Abstract

Osteoconductive function is remarkably low in bone disease in the absence of bone tissue surrounding the grafting site, or if the bone tissue is in poor condition. Thus, an effective bone graft in terms of both osteoconductivity and osteoinductivity is required for clinical therapy. Recently, the three-dimensional (3D) kagome structure has been shown to be advantageous for bone tissue regeneration due to its mechanical properties. In this study, a polycaprolactone (PCL) kagome-structure scaffold containing a hyaluronic acid (HA)-based hydrogel was fabricated using a 3D printing technique. The retention capacity of the hydrogel in the scaffold was assessed in vivo with a rat calvaria subcutaneous model for 3 weeks, and the results were compared with those obtained with conventional 3D-printed PCL grid-structure scaffolds containing HA-based hydrogel and bulk-type HA-based hydrogel. The retained hydrogel in the kagome-structure scaffold was further evaluated by in vivo imaging system analysis. To further reinforce the osteoinductivity of the kagome-structure scaffold, a PCL kagome-structure scaffold with bone morphogenetic protein-2 (BMP-2) containing HA hydrogel was fabricated and implanted in a calvarial defect model of rabbits for 16 weeks. The bone regeneration characteristics were evaluated with hematoxylin and eosin (H&E), Masson's trichrome staining, and micro-CT image analysis.

Se-Hwan Lee and Kang-Gon Lee have contributed equally to this work.

✉ Yongdoo Park
ydpark67@korea.ac.kr

✉ Young-Sam Cho
youngsamcho@wku.ac.kr

✉ Bu-Kyu Lee
bukyu.lee@gmail.com

1 McKay Orthopaedic Research Laboratory, Department of Orthopaedic Surgery, Perelman School of Medicine, University of Pennsylvania, 36th Street and Hamilton Walk, Philadelphia, PA 19104, USA

2 Department of Biomedical Sciences, College of Medicine, Korea University, 73, Goryeodae-ro, Seongbuk-gu, Seoul 02841, Republic of Korea

3 Medical Device Development Center, Daegu-Gyeongbuk Medical Innovation Foundation (K-MEDI hub), 80, Cheombok-ro, Dong-gu, Daegu 41061, Republic of Korea

4 Department of Mechanical Engineering, College of Engineering, Wonkwang University, 460, Iksan-daero, Iksan 54538, Republic of Korea

5 Biomedical Engineering Research Center, Asan Institute for Life Sciences, Asan Medical Center, 88, Olympic-ro, Songpa-gu, Seoul 05505, Republic of Korea

6 Department of Mechanical Design Engineering, College of Engineering, Wonkwang University, 460, Iksan-daero, Iksan 54538, Republic of Korea

7 MECHABIO Group, Wonkwang University, 460, Iksan-daero, Iksan 54538, Republic of Korea

8 Department of Oral and Maxillofacial Surgery, Asan Institute for Life Sciences, Asan Medical Center, 88, Olympic-ro, Songpa-gu, Seoul 05505, Republic of Korea

Graphic abstract

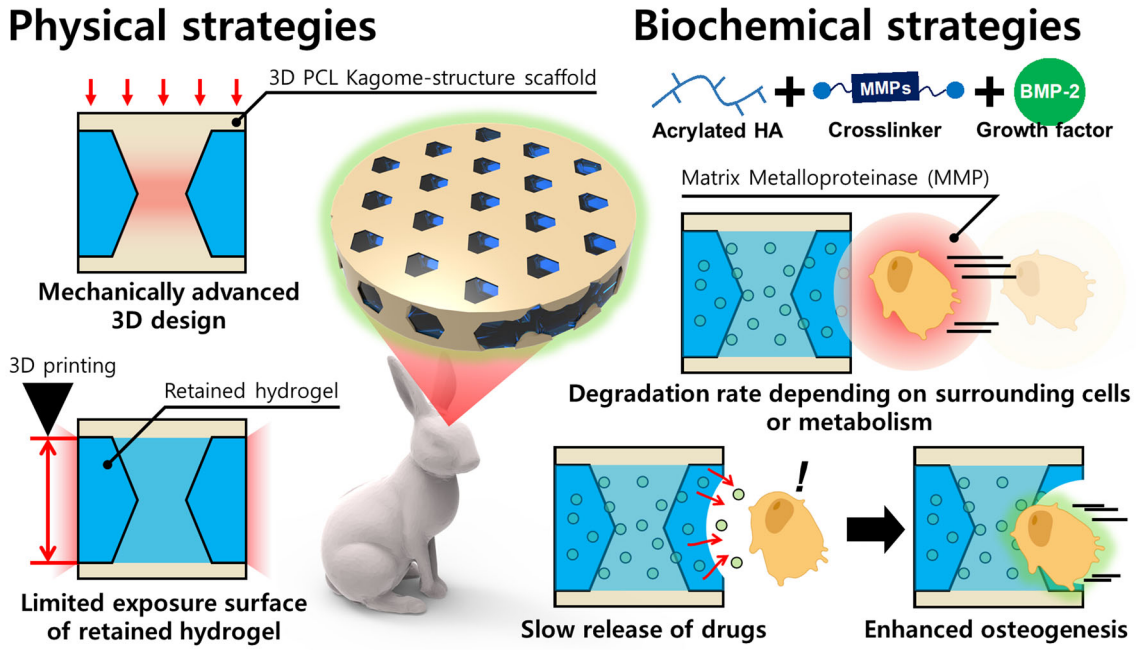

Keywords Kagome-structure scaffold · Retention capacity · Biomimetic hydrogel · Bone morphogenetic protein-2 (BMP-2)

Introduction

Bone grafts that require osteogenesis have been used for therapeutic and functional purposes due to trauma or pathological reasons. To successfully achieve osteogenesis [1, 2] in bone grafts, both osteoconduction and osteoinduction are essential. Osteoconduction involves the migration of osteoblasts from surrounding bone tissue to the bone graft site, and for this healthy normal cell source, bone cells (i.e., osteoblasts) and their progenitor cells (i.e., mesenchymal stem cells) from the tissues must be included [3]. For better osteoconduction, approaches with osteoconductive bioceramics [4] and synthetic materials [5] have been widely used for bone grafts. In addition, osteoinduction (a mechanism by which mesenchymal stem cells (MSCs) differentiate into osteoblasts after migration into bone grafts) [3] can be induced by autograft demineralized bone matrix (DBM) and bone morphogenetic proteins (BMPs) [6]. Osteoinductive growth factors could be a rational strategy for improved healing of poor bone conditions and bone regeneration around bone grafting [7, 8]. For instance, the use of BMPs can improve the osteoinductive properties of bone grafts [9]. Due to these advantages, proteins from the BMP groups are widely used for bone regeneration studies, and BMP-2 has been formally approved by the Food and Drug Administration (FDA) of the USA [10]. For clinical delivery of BMP-2, InFuse® products use acellular collagen sponge (ACS) [11, 12]. However, almost all growth factors are known to be released within 2 days [13, 14]. To facilitate the migration of osteoprogenitor cells from surrounding tissues and to differentiate them into osteoblasts, long-term sustained release of BMP-2 is required. Maintaining an appropriate concentration of BMP-2 in the recipient area is also important [15]. For this purpose, new three-dimensional (3D) printing strategies have been introduced in combination with encapsulation by microspheres [16], immobilization of molecules by surface coating [17, 18], incorporation by hydrogel concentration [19, 20], or hydrogel framework patterns [21].

Because porous structure design is a key material factor, features such as pore design, porosity, and interconnectivity of 3D scaffold are important in bone grafting, along with their biofunctions [22, 23]. Recently, Zhang et al. [24] introduced a modular-type scaffold with various pore sizes for screening osteoconduction and the osteoinduction. They confirmed that ectopic growth of bone at a pore size of 400 μm and orthotopic growth of bone at a pore size of 600 μm were promoted. Moreover, micro/nano-micropores on the surface of the bone graft could be fabricated in various forms such as regular or irregular structures and support abundant blood flow by reinforced capillary force, thereby providing smooth delivery of nutrients and the proteins required for

cell metabolism [23, 25]. In 2017, Lee et al. [26] introduced a 3D-printed polycaprolactone (PCL) kagome-structure scaffold for bone tissue regeneration as a design strategy to enhance mechanical performance of 3D scaffold, and the compressive modulus and bending modulus of the fabricated kagome-structure scaffold were respectively measured to be 1.4 times and 2.3 times higher than those of the conventional grid-structure scaffold. Based on the results of the numerical analysis, it was found that the kagome structure had a higher strain energy than the grid structure and effectively distributed the compressive stress. The grid structure was weak and had stress concentration at points where the interface between strands started to come into contact. This could be the main cause of interfacial delamination between strands of the grid structure under compressive or shear stress [27]. Recently, Cho et al. [28] showed that the mechanical properties of kagome-structured scaffolds could be enhanced up to approximately 120 MPa by fabricating them with PCL-nanosized hydroxyapatite (nHA) composite material. Osteogenic activity and bone formation were also improved by nHA particles in the composite. The 3D kagome pattern is composed of a continuous and complex pattern configured with a combination of hexagons and triangles [29]. Thus, a 3D kagome-structure scaffold design with excellent mechanical properties could be advantageous for bone tissue engineering, and well interconnected open pores based on the 3D kagome pattern could provide space as a container to deliver hydrogels with bioactive cues. The hydrogel could protect the encapsulated cells during 3D multi-printing with a high melting temperature-head as well as provide a suitable environment for the cells [30, 31]. Moreover, the hydrogel can contain soluble bioactive proteins for sustained release [18]. For these reasons, incorporating protein-based bioactive factors such as BMP-2 and BMP-7 into hydrogels in synthetic polymeric scaffolds could be an effective strategy to enhance the osteoinductive potential of bone grafting. In matrix metalloproteinase (MMP)-sensitive HA, cultured human mesenchymal stem cells (hMSCs) with low molecular weight (50 kDa) showed high viability for 3 days in vitro, which was a clear improvement compared to those with high molecular weight (200 kDa). When compared with a group to which integrin-binding domains (Arg-Gly-Asp: RGD) peptide was added, cell proliferation analysis showed similar levels [32]. For the PCL kagome-structure scaffold, the results for cell proliferation and DNA contents in vitro revealed that the PCL kagome scaffold was superior to the PCL grid scaffold, and it was found that smooth adhesion of early cells could be induced by the surface roughness and wrinkles of the kagome scaffold [26]. Therefore, both the PCL and MMP-sensitive HA, as main materials of our scaffold, have been evaluated as materials with excellent cell adhesion and very low cytotoxicity. However, there has not been satisfactory analysis of the causes that induce slow release of BMP-2 based on pore morphology and stimulus-responsive hydrogels in 3D-printed scaffolds. Therefore, it is still necessary to analyze the cause of the slow release of BMP from the scaffold in vivo [33].

In this study, PCL kagome-structure scaffold with BMP-2 containing hyaluronic acid (HA) based hydrogel was fabricated by a 3D printing technique for bone regeneration. In addition, we analyzed the geometrical and morphological characteristics of the fabricated scaffold compared with a conventional 3D-printed grid-structure scaffold. To evaluate the in vivo retention capacity of the HA-based hydrogel in the scaffold, both kagome-structure and conventional grid-structure scaffolds were implanted subcutaneously into rat calvaria for 3 weeks. In addition, to assess in vivo new bone formation with the fabricated PCL kagome-structure scaffold made of BMP-2/HA-based hydrogel, the scaffold was implanted in a calvarial defect model in rabbits for 16 weeks.

Materials and methods

Materials

We used PCL (M_n=45,000, T_m=60 °C, Sigma-Aldrich, St. Louis, MO, USA) to fabricate 3D porous scaffolds for transplantation in animals. CATIA V5 R13 software (Dassault systems CATIA, France) was utilized to design the 3D scaffolds. A digital scale (HS204, Hansung, Republic of Korea) with 0.1 mg resolution was used to measure the weight of the scaffold. To measure pore size, an optical microscope (Mi-9100 ZOOM(S), Magic i, Republic of Korea) was used. Sodium hyaluronate (Mw: 60 kDa, Korea University, Republic of Korea) was purchased from Lifecore Biomedical. 1-Ethyl-3-(3 dimethylaminopropyl) arbodiimidee (EDC), adipic acid dihydrazide (ADH), and triethanolamine (TEA) were acquired from Sigma-Aldrich (USA). 1-Hydroxybenzotriazole hydrate (HOBT) was purchased from Fluka Chemical (Buchs, Switzerland). N-acryloxysuccinimide (NAS) was purchased from Polyscience (Warrington, USA). Substance P (RPKPQQFFGLMC), matrix metalloproteinase (MMP)-sensitive peptide (GCRDGPQGIWGQDRCG) was synthesized by Anygen (Gwangju, Republic of Korea). Flamma-675 (BCT-PWS1515-M001, Bioacts, Republic of Korea) fluorescence and BSA (15,561,020, Thermo Fisher Scientific, USA) were mixed with hyaluronic acid hydrogel (5 wt%) and used for in vivo imaging system (IVIS) scanning (IVIS 200, Xenogen Corporation, USA) to quantify hydrogel retaining ability. Carrier-free recombinant human BMP-2 was purchased from R&D Systems (USA).

Preparation of biomimetic HA-based hydrogel

To prepare HA-based hydrogels degradable by secreted MMP in cells, HA was acrylated as in previous studies [34]. The acrylated HA was dissolved in the buffer, and the MMP-sensitive peptide was added in the same molar ratio to the acrylic group and thiol group. The HA-based hydrogel was formed via a Michael-type addition reaction.

Fabrication of customized PCL kagome-structured scaffolds with HA-based hydrogels and BMP-2

To fabricate customized scaffolds for an 8-shaped defect model, we utilized individually collected medical image data for all populations as design references and carried out the fabrication process according to the description in a previous study [27]. The medical images of the 8-shaped defect model of the rabbit were acquired by computed tomography (CT). We designed the 3D kagome-structure model (with a height of 1.2 mm and porosity of approximately 50%) using CATIA software. The model was assembled using the 3D defect model reconstructed from the CT images, and an outline of the assembled kagome model was modified to fit the defect morphology. A tailored 3D kagome model was exported in stereolithography (STL) format. This STL file was sliced using a slicing engine of the open-source software Slic3r (version 1.2.9), and raw g-code data were generated. During the execution of the g-code, for the path of the PED (precision extracting deposition) head that fabricates the PCL part of the scaffold, we predefined the nozzle size and infill density to be 50 μm and 100%, respectively. For the path of the syringe pump head that fabricates the hydrogel part of the scaffold, we set the nozzle size and infill density to 500 μm and 100%, respectively. To automatically calibrate command errors that occur between the raw g-code and motion control software, the raw g-code was converted to a calibrated g-code by in-house program.

A laboratory-made 3D printer with a PED head and syringe pump heads was used to fabricate a scaffold with multiple materials. PCL material was melted in a barrel at 80 °C. The melted PCL material was input into the cartridge body in the PED head with (313±5) kPa air pressure. The temperature of the cartridge body and ceramic nozzle were maintained at 80 °C, and the melted PCL was extruded through a ceramic nozzle by a rotating screw at 70 rpm in the cartridge body. The ceramic nozzles used for fabrication of the PCL kagome-structure scaffold and the PCL grid-structure scaffold were 50 μm and 400 μm, respectively. The HA-based hydrogel was extruded by a syringe head with a 500 μm inner-diameter needle. A heating bed was maintained at 37 °C. We fabricated the PCL kagome-structure scaffold with an HA-based hydrogel with BMP-2 (20 μg/mL) using these processes.

Characterization of fabricated PCL scaffold

In order to assess the in vivo retention capacity of the hydrogel in subcutaneous rat calvaria, we designed kagome- and grid-structure scaffolds with predefined cylindrical shapes, as shown in Figs. 1a and 1b. These scaffolds were fabricated with a 3D printer with a PED head, as shown in Figs. 2a and 2b, respectively.

Equation (1) was used to define the pore size of the scaffold as follows:

$$\text{Pore size } (\mu\text{m}) = \frac{L_\text{v} + L_\text{h}}{2}, \tag{1}$$

where L_v and L_h are the lengths of the pores measured in the vertical and horizontal directions, respectively. Pore size was calculated by averaging the L_v and L_h values (n=5) measured by optical microscopy.

Equation (2) was used to calculate the porosity of the scaffold:

$$\text{Porosity } (\%) = \frac{V_0 - \frac{m_\text{s}}{\rho_\text{PCL}}}{V_0} \times 100, \tag{2}$$

where V_0 is the calculated volume from the apparent dimensions of the scaffold, ignoring pores. m_s and ρ_PCL are the mass of the scaffold and the density of the PCL material (1.145 g/cm^3).

Evaluation of cell viability and proliferation in vitro

To assess cell culture characteristics of the fabricated scaffolds in vitro, we predefined in vitro experimental groups as follows: Group-I and Group-II are grid-structure scaffold and kagome-structure scaffold (w/o HA-based hydrogel or BMP-2), respectively. Group-III is the PCL kagome-structure scaffold with HA-based hydrogel, and group-IV is the PCL kagome-structure scaffold with HA-based hydrogel containing BMP-2, as depicted in Table S1 (Supplementary Information). For Group-I and Group-II, the fabricated scaffolds were washed with 70% EtOH and sterilized under ultraviolet (UV) light for 1 h. In Group-III and Group-IV, the fabricated scaffolds were only sterilized under UV light for 1 h. Prior to the in vitro experiment, all groups were prewetted in phosphate buffered saline (PBS) for 1 h. Saos-2 (Osteosarcoma, P.3) cells were seeded at 5×10^5 cells per scaffold. After 30 min, low glucose Dulbecco's modified Eagle's medium (DMEM, Gibco, USA), supplemented with 10% fetal bovine serum (FBS) and 1% penicillin (P/S), was added to allow the cells to attach to the scaffold and this was observed for 14 days. Live/dead staining (Calcein AM and Ethidium homodimer-1, Thermo Fisher, USA) was performed on 1, 7, and 14 days. Cell counting Kit-8 (CCK-8, Dojindo, Kumamoto, Japan) was used on days 1, 3, 7, and

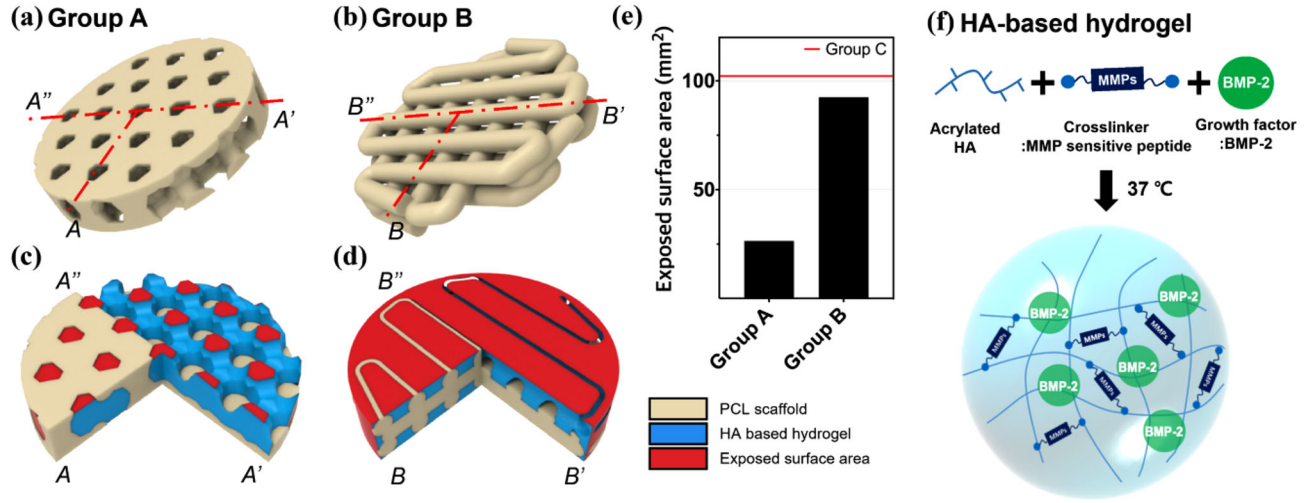

Fig. 1 Illustration of the polycaprolactone (PCL) framework: **a** kagome-structure scaffold, **b** grid-structure scaffold; cross-sectional illustration: **c** kagome-structure scaffold (beige) with hydrogel (blue), **d** grid-structure scaffold with hydrogel; **e** exposed surface area (red), **f** synthesis of acrylated HA gel

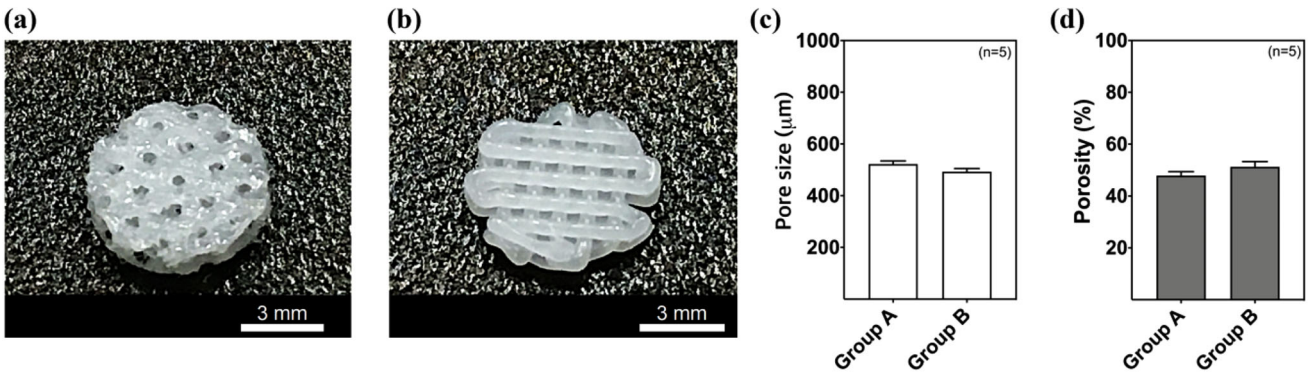

Fig. 2 Fabricated polycaprolactone (PCL) scaffolds: **a** Group A, **b** Group B; **c** measured pore size (n=5), **d** measured porosity (n=5)

14. The images were captured at a 10× magnification with a fluorescence microscope (Nikon, Ti2-E, Tokyo, Japan), and a microplate reader (Thermo Fisher VarioskanTM LUX, Waltham, MA, USA) was used for absorbance measurement.

IVIS scanning for quantification of hydrogel-retaining capacity

To compare the retaining capacity of the hydrogel in the fabricated PCL scaffolds, we extruded 30 μL HA-based hydrogel in the PCL scaffolds with a multihead printing technique, as discussed in Section "Fabrication of customized PCL kagome-structured scaffolds with HA-based hydrogels and BMP-2". After extruding the hydrogel, we performed gelation in a 37 °C incubator for 30 min and implanted the hydrogel subcutaneously into rat calvaria; we then observed the experiment for 3 weeks. For rat calvarial implantation, 6-week-old rats (Orient Bio, Republic of Korea) were approved by the Institutional Animal Care and Use Committee (IACUC) and acclimatized in the breeding room for 1 week. They were then used for in vivo experimentation. After intramuscular (IM) anesthesia with zoletil (15 mg/kg) and xylazine hydrochloride (3.5 mg/kg), rat calvarial hair was shaved. After that, povidone-iodine solution was used for sterilization, and a 5-cm incision was made in the skin. After implantation of the fabricated scaffold with HA-based hydrogel subcutaneously in rat calvaria, the skin layer was sutured and observed once a week using an IVIS imaging system (IVIS 200, Xenogen, USA).

To calculate the degradation rate, the projected area after implantation was used with respect to the initial value. The relative unit value of the projected area with respect to implantation time was calculated using the initial projected area. Next, we defined a linear equation for each group using a simple linear fitting algorithm. The degradation rate was calculated by differentiating the obtained linear equation.

Animal preparation and surgical process for bone regeneration

Approval for this experiment was obtained from the IACUC of the Asan Medical Center, University of Ulsan College of Medicine (Republic of Korea). New Zealand White rabbits (Orient Bio, Inc., Republic of Korea) weighing approximately 2.5 kg (12–13 weeks old) were used and allowed a 1-week acclimatization period inside the cage prior to surgery. The animals were anesthetized by intramuscular injection of Zoletil (15 mg/kg) and xylazine hydrochloride (3.5 mg/kg). Their scalps were shaved and scrubbed with a povidone-iodine solution to avoid contamination. After subcutaneous injection of local anesthetic (lidocaine hydrochloride with epinephrine 1:100,000) for hemostasis and pain reduction, we exposed the calvarium with an approximately 1.5 cm sagittal midline scalp incision using a sterilized scalpel so that the bregma (an intersection point of the coronal suture and sagittal suture perpendicularly) lay in the center of the opening.

To create a bone defect at a specific position, we held the initial defect position at 2 mm in front of the lambdoid suture line of the calvaria. To create an 8-shaped defect, the 8 mm circle was overlapped by approximately 1 mm. A bone defect was created symmetrically with respect to the sagittal suture line (2 mm apart) to produce the same 8-shaped defect on the other side. The complex bone defect was designed into an 8-shaped structure using two circles of the same size with a diameter of 7 mm.

Any debris or bone chips remaining were irrigated with sterile normal saline, and the periosteum and skin were closed separately with 3–0 polypropylene sutures and scrubbed with povidone-iodine solution. After the operation, computed tomography images of the calvarium were taken (CT; Siemens, Germany), and postoperative management was conducted by intramuscular injection of ampicillin (50 mg/kg) and ketorolac tromethamine (1 mg/kg) twice a day for three days to prevent infection and pain, respectively.

CT scanning

CT scanning was performed on the calvarial bone at 1, 2, 4, 8, 12, and 16 weeks following implantation. The animals were killed at 4, 8, 12, and 16 weeks after implantation. Images were acquired using a 16-slice multidetector CT scanner (SOMATOM Sensation 16, Siemens AG, Forchheim, Germany). Parameters for CT acquisitions were adapted as follows: tube voltage, 120 kV; current intensity, 220 mA; slice thickness, 0.75 mm. The in-plane resolution of this CT protocol was estimated at 0.4 mm×0.4 mm. Axial slices (0.1 mm thick) were reconstructed on the scanner with an H60s medium-smooth kernel. The field of view was 100 mm×100 mm, and the data were acquired in a 512×512 data matrix.

Bone-volume analysis

Using the CT data, the threshold and region of interest were set to 8-shaped defects with a diameter of 8 mm. After selecting a 1.0 mm thickness for measurement, the amount of new bone volume was measured with ImageJ software plug-in package (National Institutes of Health, USA). Equation (3) was used to define the new bone formation as follows:

$$\text{New bone formation}\,(\%) = \frac{V_{\text{nb}}}{V_{\text{d}}} \times 100, \tag{3}$$

where V_{d} is the 3D volume of the initial defect for each animal and V_{nb} means the 3D volume of the newly formed bone within defect region at predefined time. The new bone formation was calculated by averaging five samples.

Histology

After killing, samples were immediately fixed with 4% (w/v) paraformaldehyde. Fixation was performed for 5 days, and the fixed samples were decalcified in 10% ethylenediaminetetraacetic acid (EDTA) for 30 days at room temperature. The decalcified samples were embedded in paraffin after dehydration. Paraffin blocks were stained with hematoxylin and eosin (H&E) and Masson's trichrome by the manual method after 3-μm-thick sectioning. H&E and Masson's trichrome staining were performed using the basic protocol. In the Masson's trichrome images, the stained area in the scaffold was used to analyze mineralized bone density and collagen density, and quantification was performed with ImageJ software.

Statistical analysis

All data are indicated as the mean±standard deviation. The statistical analysis for Figs. 3c and 4b was conducted using single-factor analysis of variance (ANOVA) via SPSS version 22.0 software (SPSS, IBM Corporation, Chicago, IL, USA). The statistical analysis for Figs. 6b and 6c (which will be shown later) was performed with two-way ANOVA via GraphPad Prism version 9 software (San Diego, CA, USA). A value of $p<0.05$ was considered statistically significant.

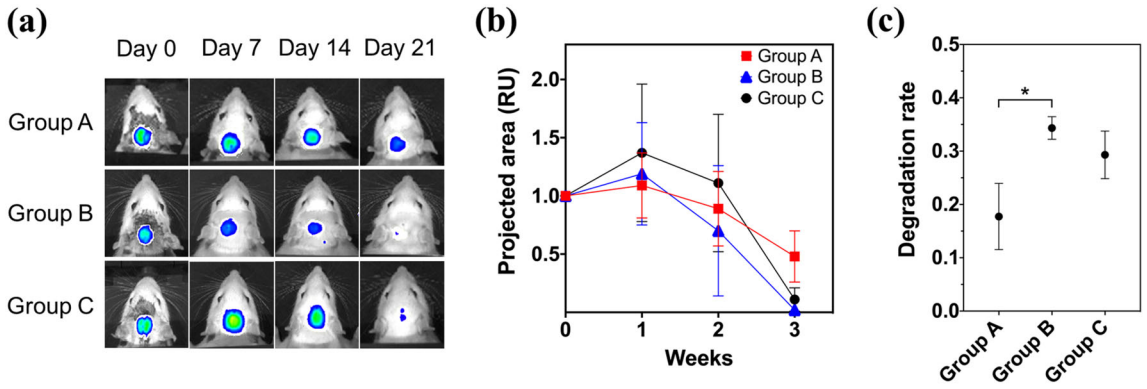

Fig. 3 **a** In vivo imaging system (IVIS) images after implantation (n=3), **b** relative unit value of projected area based on IVIS image data, **c** calculated degradation rate (*p<0.05)

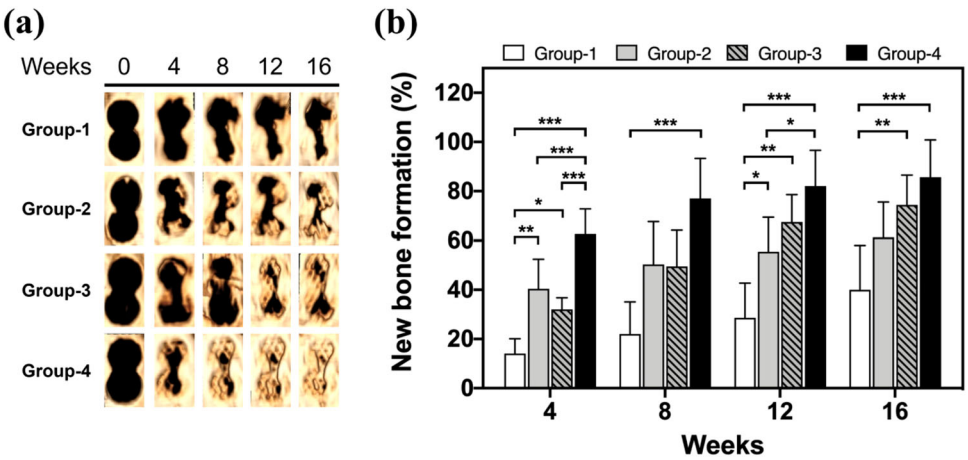

Fig. 4 **a** 3D live CT images, **b** new bone formation graph (*p<0.05, **p<0.01, ***p<0.001)

Table 1 Experimental groups for rat in vivo tests under subcutaneous tissue

Group	Scaffold	HA-based hydrogel
Group A	Kagome-structure	+
Group B	Grid-structure	+
Group C	–	+

Results

Geometrical characteristics of the designed scaffolds

To assess the degradation rate of the HA-based hydrogel in the fabricated scaffold with respect to implantation time, we determined the experimental groups as follows: Group A and Group B were defined as the kagome-structure scaffold and the grid-structure scaffold with HA-based hydrogel, respectively. Group C was defined as the bulk-type HA-based hydrogel, as depicted in Table 1.

Group A and Group B were designed to have similar pore sizes and porosities, as shown in Figs. 1a and 1b. The predefined pore size and porosity of Group A were designed to be 620 μm and 48.61%, respectively. Those of group B were designed to be 530 μm and 52.18%. A local cross-sectional illustration is shown in Figs. 1c and 1d for each scaffold containing hydrogel that was assembled to ideal specifications with CAD software. To indicate the cross section of each design, the 3D models were cut in the A-A' and B-B' regions. In the A'-A" and B'-B" regions, only half of the PCL scaffold (beige-colored) was removed in the thickness direction to exhibit the complex morphology of the HA-based hydrogel loaded in each PCL scaffold. The exposed surface area of the hydrogel model in the scaffold in the early stage of degradation after transplantation is shown in red in Figs. 1c and 1d. Each group was quantitatively analyzed, as shown in Fig. 1e. The exposed areas of Group A, Group B, and Group C were calculated to be 26.43, 92.45, and 102.2 mm^2, respectively.

We used 3D geometrical models of the kagome-structure scaffold and grid-structure scaffold with similar porosity and pore size to analyze the geometrical difference. As

shown in Fig. 1e, the exposed surface area of Group A was approximately 3.5 times less than that of Group B. The exposed surface area of the hydrogel was significantly different between Groups A and C. The relative values of the exposed surface area of Groups A and B with respect to Group C were 0.26 and 0.90, respectively. The hydrogel exposure level of Group A was designed to be approximately 26%, which confirmed that the Group A was designed to be approximately 3.5 times less than that of Group B.

Morphology of the fabricated scaffolds

The scaffolds for Group A and Group B that were fabricated using 3D printing are shown in Figs. 2a and 2b. The Group A scaffold had a diameter of (6.89±0.04) mm and thickness of (1.50±0.03) mm (n=5). That of Group B was fabricated to have a diameter of (6.85±1.28) mm and thickness of (1.28±0.04) mm (n=5). As depicted in Fig. 2c, Groups A and B had pore sizes of (522.32±11.89) μm and (492.94±12.00) μm, respectively. As shown in Fig. 2d, the porosity of Groups A and B was (47.90±1.47)% and (51.27±2.03)%, respectively. The scaffolds were fabricated to have similar pore sizes and porosities. In a previous study, the mean relative errors of the fabricated kagome scaffold and grid scaffold were analyzed to be 2.6% and 5.0% [35], which means that they were fabricated with 97.4% and 95.0% accuracy compared with the 3D design models.

Evaluation of cell viability and proliferation in vitro

The Saos-2 cells were cultured on the surface of the fabricated scaffolds in vitro for 14 days. Live/dead staining was performed to assess the cytotoxicity of the fabricated scaffolds. As shown in Fig. S1 (Supplementary Information), the number of dead cells observed was insignificant in all groups and high viability of the attached cells was maintained for 14 days. A CCK-8 assay was carried out to analyze cell viability and proliferation over 14 days. As shown in Fig. S2 (Supplementary Information), increased cell viability and proliferation of the attached cells on the scaffold were measured in all groups; the proliferation rate of Group-IV was also slightly higher than that of other groups.

In vivo degradation characteristics of HA-based hydrogels loaded in PCL scaffolds, as measured by IVIS analysis

To assess the in vivo degradation characteristics of HA-based hydrogels in PCL scaffolds, we subcutaneously transplanted the fabricated scaffolds for each group into rat calvaria. After transplantation, the IVIS test was carried out for 3 weeks. As depicted in Fig. 3a, the projection area for each group decreased with respect to the implantation time. The HA-based hydrogel was observed to degrade from the outer region to the center region. For each group, the relative unit value of the projected area was quantitatively analyzed, as shown in Fig. 3b. Based on this result, the degradation rate was analyzed for the full transplantation period, as shown in Fig. 3c. The calculated degradation rates for Groups A, B, and C were 0.18±0.06, 0.34+0.02, and 0.29±0.05, respectively.

Table 2 Experimental groups for the in vivo test using rabbit calvarial defects

Group	Kagome-structure scaffold	HA-based hydrogel	BMP-2
Group-1	Nonimplanted defect model	−	−
Group-2	+	−	−
Group-3	+	+	−
Group-4	+	+	+

Assessment of new bone formation with micro-CT analysis

To assess the osteogenesis of the PCL kagome-structure scaffold with HA-based hydrogel containing BMP-2, in vivo experimental groups were predefined as follows: Group-1 had a nonimplanted defect model as a negative control group, Group-2 had the PCL kagome-structure scaffold (w/o HA-based hydrogel or BMP-2) as a control group, Group-3 had the PCL kagome-structure scaffold with HA-based hydrogel, and Group-4 had the PCL kagome-structure scaffold with HA-based hydrogel containing BMP-2, as depicted in Table 2. In Fig. 4b, the respective new bone volumes in Group-1 and Group-2 were (14.09±6.02)% and (40.43±11.99)% after four weeks, (22.03±13.07)% and (50.33±17.29)% after eight weeks, (28.63±14.09)% and (55.44±13.98)% after 12 weeks, and (40.01±17.99)% and (61.27±14.35)% after 16 weeks. The respective new bone volumes in Group-3 and Group-4 were (32.01±4.74)% and (65.59±10.21)% after four weeks, (49.51±14.64)% and (77.02±16.25)% after eight weeks, (67.46±11.10)% and (82.07±14.54)% after 12 weeks, and (74.42±12.14)% and (85.64±15.12)% after 16 weeks.

Histological analysis

In the histological evaluation shown in Fig. 5, serious inflammation or infection was not observed at the graft site for 16 weeks. As seen in the figure, newly formed bone was observed with Masson's trichrome staining in all groups at 4 and 16 weeks. In Group-3, woven bone and extracellular

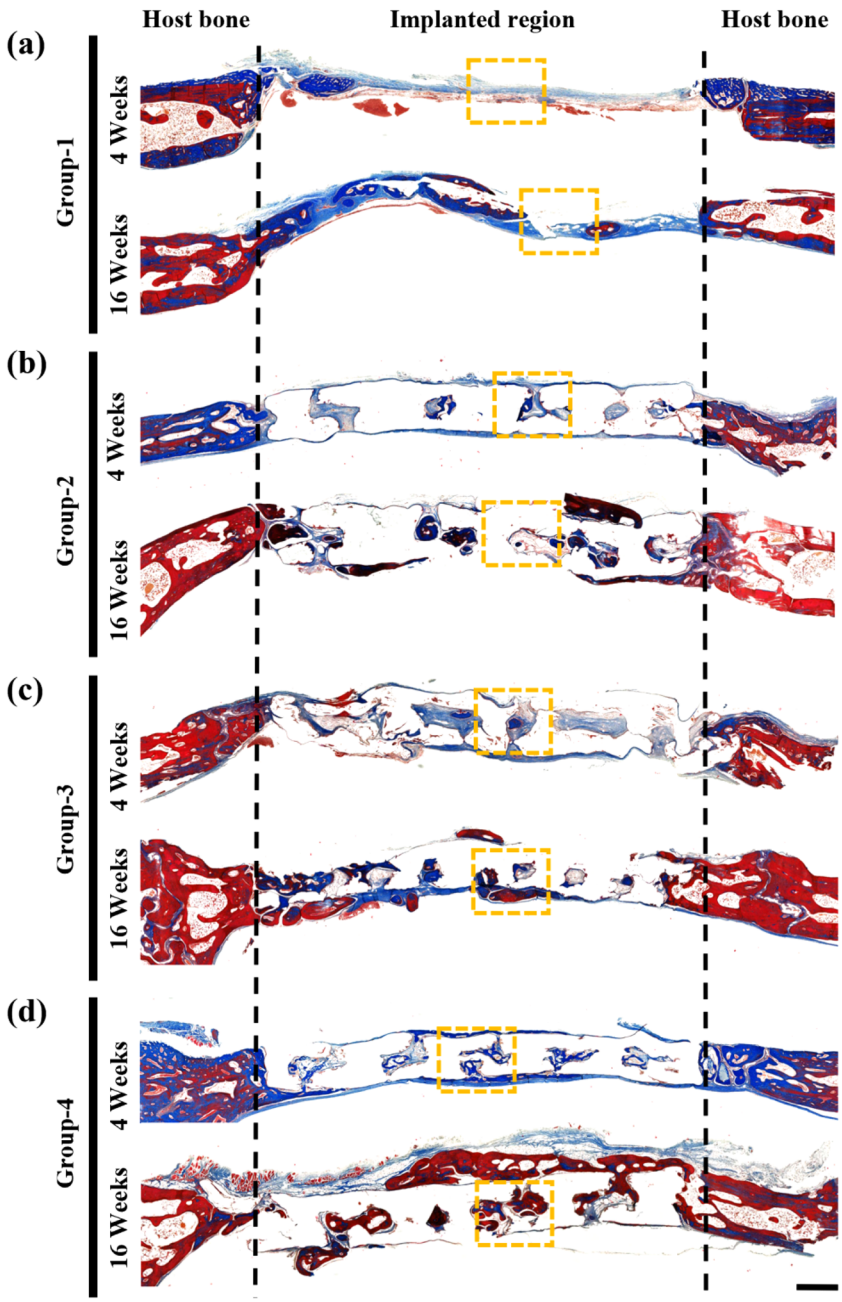

Fig. 5 Histologic evaluation was performed on the rabbit calvaria defect model at 4 and 16 weeks with Masson's trichrome staining (1.25×). The black dotted lines indicate the area where the kagome-structure scaffold was implanted, and the yellow dotted lines indicate the region of the magnified images; **a** Group-1: non-defective implanted model, **b** Group-2: kagome-structure scaffold, **c** Group-3: kagome-structure scaffold with HA-based hydrogel, and **d** Group-4: kagome-structure scaffold with BMP-2/HA-based hydrogel (scale bar: 1 mm)

matrix (ECM) were observed. The woven bone formed in large regions inside the scaffold in Group-4. Moreover, we confirmed that mineralized bone had formed at 16 weeks inside the scaffold that was loaded with BMP-2/HA-based hydrogel. In Fig. 6, histologic findings for Group-3 show that osteoblasts and osteocytes were significantly activated around the bone marrow tissue. The newly formed bone in Group-3 was immature compared with that in Group-4, meaning that new bone formation in Group-4 could be generated more actively than in Group-3. As depicted in Fig. 6, lamellar bone was observed at 16 weeks in Group-2, Group-3, and Group-4. In addition, mineralization was evident around the blood vessels in the center of the newly formed bone tissue.

Discussion

In this study, we loaded an HA-based hydrogel containing BMP-2 in the PCL kagome-structure scaffold to support the osteoinductive effect for bone regeneration. Theoretically, when the hydrogel in the scaffold is implanted in the body, the hydrogel degrades with time due to the physiological environment surrounding the scaffold [36]. The

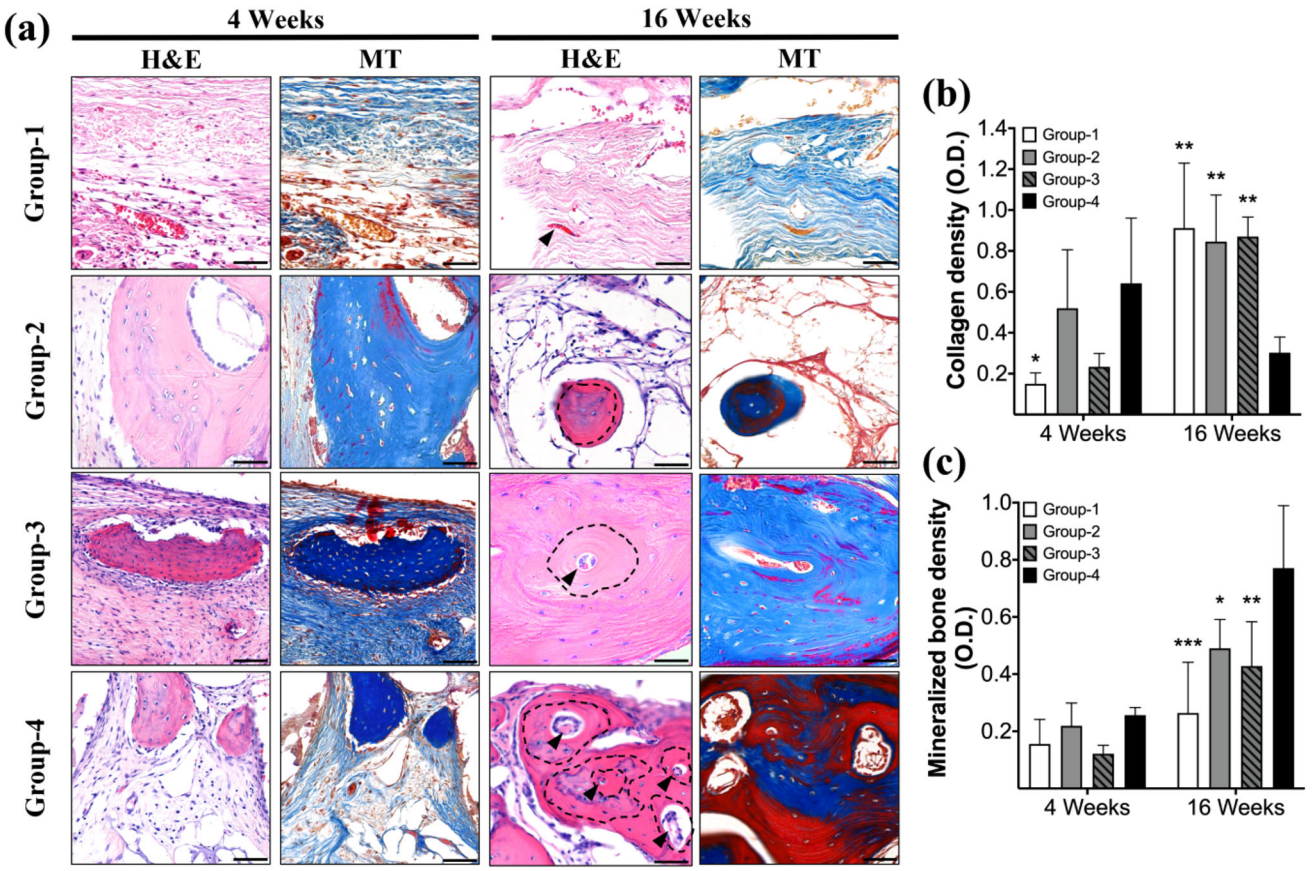

Fig. 6 H&E and Masson's trichrome staining were carried out at 4 and 16 weeks of the rabbit calvarial defect model (40×). **a** The black arrows indicate the regions of the blood vessel, and the black dotted lines indicate the lamellar bone (scale bar: 100 μm), **b** collagen density, and **c** mineralized bone density (n=4, $^{*}p$<0.05 vs. Group-4, $^{**}p$<0.01 vs. Group-4, $^{***}p$<0.001 vs. Group-4)

HA-based hydrogel applied in this study has the characteristic of stimulus-responsive degradation. In other words, because it is degraded by MMP secreted from cells, the level of degradation can depend on the level of exposure to surrounding cells [37]. Degradation of hydrogels by MMP is known to regulate cell survival and differentiation and also plays an important role in tissue regeneration and remodeling [38]. In addition, one can induce migration of cells required for tissue regeneration into the hydrogel [39]. The migrated cells act continuously as the main source of hydrogel degradation and promote cell adhesion and delivery of nutrients necessary for cells. At the same time, differentiation of stem cells into bone cells is induced by the release of BMP-2 incorporated in the hydrogel [40]. However, at least 4 weeks are required for successful osteoinduction by controlled release of BMP-2 at the region for regeneration [41].

To induce slow release of the growth factor, the approach of using only hydrogel could be markedly more sensitive in controlling physicochemical properties [42]. Several patterned structures of the 3D scaffold could affect the degradation characteristics of contained HA-based hydrogel. The geometry of the hydrogel in the scaffold depends on the shape of the inner pores. Therefore, the exposure level of the hydrogel to surrounding tissue is related to the area or exposure morphology of the scaffold pores. In the case of a grid-patterned scaffold containing hydrogel, the hydrogel can be contained by adjusting the distance between the strands [43, 44]. However, this could be a pattern that is unable to produce a long drug release time for a design that features a large exposed area of the contained hydrogel. As shown in Figs. 1c and 1d, the kagome structures cover a significant surface area of the hydrogel compared with the grid structure, while the exposed area is limited, as depicted in Fig. 1e. This means that the exposed surface area of the hydrogel contained in the scaffold can be effectively controlled by the 3D printing technique. On the other hand, the hydrogel exposure level of Group B was confirmed to be approximately 90%. This means that there was not a significant difference between Group B and Group C. This result could be caused by a high degradation rate of the hydrogel in the early stages of implantation. Therefore, the design of the kagome-structure scaffold could be

more advantageous than a conventional grid-structure scaffold as a container for inducing delayed degradation of the HA-based hydrogel, which could lead to slow release of the BMP-2 contained in the HA-based hydrogel. Additionally, since HA-based hydrogels with the aforementioned stimulus-responsive degradation characteristics have a degradation rate dependent on the tissue regeneration rate, burst degradation of the HA-based hydrogels could be prevented while also being ideal for tissue regeneration [34]. Because we considered both physical and biochemical strategies, it was possible to achieve slow release in vitro for at least three weeks, a length of time which is effective at bone regeneration sites where growth factors are required. In the results of the in vitro test, although there were no statistically significant differences between groups over the short periods considered here, cell proliferation in Group-IV was slightly better compared with other groups, and the addition of HA or BMP did not negatively affect cell viability and proliferation (see Figs. S1 and S2 in Supplementary Information). This may mean that the burst release of the drug contained in Group-IV did not occur during the in vitro culture period; another possible cause is the absence of metabolism in the in vitro microenvironment. Therefore, the developed is suitable for in vivo transplantation of the developed scaffolds, and long-term in vivo experiments could be more suitable for identifying differences between groups.

In the in vivo environment, as the MMP-sensitive peptide acting as the cross-linker in the HA-based hydrogel is broken by surrounding cells, the stiffness of the hydrogel gradually decreases. This can cause swelling of the hydrogel at the early stage of implantation. The swelling of the hydrogel allows more inflow of soluble factors (such as the MMP) and more cell migration. Eventually, degradation of the hydrogel is promoted. The volume of HA-based hydrogel in all groups increased in the projected area after 1 week (see Figs. 3a and 3b). We assume that this is due to the influence of the swelling properties of the HA-based hydrogel. Kim et al. [34] showed that HA-based hydrogels in vitro can have swelling ratios above 200%. We analyzed the increase in the projected area due to swelling and found that Group C had the highest increasing slope and Group A had the lowest. Therefore, the degree of swelling in the HA-based hydrogel at the early stage of implantation depends on the exposed surface area of the scaffold, which depends on the scaffold design. The degradation profile of the HA-based hydrogel could be related to the release profile of drugs encapsulated in the hydrogel [45]. As shown in Fig. 3c, the degradation rates of Group B and Group C were not significantly different, and most of them were degraded 3 weeks after implantation. On the other hand, Group A had the lowest degradation rate of approximately 51.7% in comparison with Group B. Although Groups A and B had similar porosities, their degradation rates were significantly different. That can be understood as a characteristic of 3D pore design structure which was more open to surrounding tissue in Group B. Diffusion of the internal material in the grid-structure scaffold can occur relatively quickly. In Group A, the morphology of the interconnected pores could be described as a structure that induces a low degradation rate of the hydrogel with respect to implantation time. Consequently, the slow degradation rate of the HA-based hydrogel in the PCL scaffold in vivo could be induced by the high hydrogel-retaining capacity of Group A. Because of the degradation characteristics of the hydrogel, the components in the HA-based hydrogel contained in the kagome-structure scaffold can be released slowly compared to release that from the grid scaffold relatively. Minimizing the diffusion rate of BMP-2 from the delivery system is known to be desirable for bone-tissue regeneration [46]. Moreover, the custom-fitting ability of the kagome-structure scaffold has been shown to be superior to that of the grid-structure scaffold [27]. For these reasons, the kagome scaffold structure can be described as a progressive design that could provide enhanced bioactive function compared with the conventional grid-structure scaffold for bone-tissue engineering.

Growth factors required for tissue regeneration are secreted and applied differently at each stage. For example, BMP-2 or BMP-4 is secreted during the initial 2 weeks required for bone regeneration [47, 48]. To increase its bone regeneration effect, it is necessary to maintain the growth factor at the regeneration site for 4 weeks [49]. However, there have been reports of problems with initial burst release in which 95% of the growth factors are released within the initial 2 weeks in materials used in clinical treatment [50–52]. In the in vivo new bone formation results, the bone regeneration of the kagome-structure scaffold loaded with BMP-2 was significantly faster, as shown in Figs. 4a and 4b. Not only was the new bone formation of Group-4 approximately 4.4-fold, 1.5-fold, and 2.0-fold higher, respectively, than that of Group-1, Group-2, and Group-3 at 4 weeks, but we also confirmed that most of the defect space had already been filled with newly created bone at week 8. In Group-4, a similar trend can be seen in the in vitro experimental result (Group-IV in Fig. S2 in Supplementary Information). In addition, the influence of abundant cells and metabolism around the implantation site in the body could have affected growth-factor release in Group-4. Figure 6a shows that the amount of initial bone formation was successfully enhanced by retaining the BMP-2/HA-based hydrogel for at least 3 weeks. As depicted in Figs. 4b and 6b, both the initial bone formation and collagen density are high. We confirmed that there was much mature bone formation at 16 weeks (Fig. 6c); thus, evaluating the bioactive effect of the fabricated systems, such as Group-III and Group-IV, could be advantageous for reconstruction of large-volume defects. In a previous study [28], kagome-structure scaffold using the PCL/bioactive ceramic

composite did not show a clear difference from the defect group at the 4th week. Thus, the scaffold developed in this study appears to be very effective for bone regeneration. According to Ku et al. [33], the rate of new bone formation in the PCL kagome scaffold implanted as an onlay graft on rat calvarial bone can be boosted by an HA-based hydrogel system with BMP-2 (HA/BMP-2). However, they suggested that it would be advisable to analyze the effect of slow-release BMP-2 from a kagome-structure scaffold system with the HA/BMP-2. In this study, it was proved that the kagome-structure scaffold including HA-based hydrogel with BMP-2 is significantly effective for bone regeneration, from both the design and material points of view. In future studies, it may be necessary to develop mechanical performance similar to the surrounding tissue by applying a bioceramic-polymer composite material, and to develop a vascular induced scaffold (essential for large-area bone reconstruction) by adding angiogenic growth factors into the hydrogel system.

Conclusions

In this study, we induced a slow release rate of growth factor using both the geometrical strategy of a 3D scaffold and the chemical strategy of an HA-based hydrogel with MMP-sensitive peptide. To enhance osteoinductivity, we fabricated PCL kagome-structure scaffold with BMP-2/HA-based hydrogel, using a 3D printing technique. Based on our results, we would like to highlight the following key characteristics of the fabricated kagome-structure scaffold for bone regeneration. First, the hydrogel is better retained in the kagome-structure scaffold than in the conventional grid-structure scaffold. In terms of drug delivery, the kagome-structure scaffold could be structurally advantageous. Second, kagome-structure scaffolds loaded with BMP-2/HA-hydrogel effectively induce new bone formation. In particular, the induced osteogenesis performance is maintained at a high level from the early stage. As a remaining challenge, further research could be done on inducing sustained release of bioactive factors for more than 4 weeks by controlling the pore design or hydrogel properties; this would allow customization for various types of patients.

Supplementary Information The online version contains supplementary material available at https://doi.org/10.1007/s42242-022-00219-x.

Acknowledgements This research was supported by the Korea Health Technology R&D Project through the Korea Health Industry Development Institute (KHIDI), the Ministry of Health & Welfare, Republic of Korea (Grant Number: HI14C2143), and the National Research Foundation of Korea (NRF) grant funded by the Korea government (MIST) (NRF-2021R1A2C2009665). We thank the Laboratory of Animal Research core facility at the ConveRgence mEDIcine research cenTer (CREDIT), Asan Medical Center for support and instrumentation.

Author contributions SHL, KGL, JL, YP, YSC, and BKL contributed to conceptualization; SHL, KGL, and JL contributed to writing-original draft preparation and visualization; JL and KGL contributed to synthesis of HA-hydrogel system; SHL, YSC, and MSG contributed to 3D printing; KGL and SK contributed to animal experiment; SHL, KGL, and JL contributed to analysis of experimental results; SHL, KGL, SJH, YP, YSC, and BKL contributed to review and editing; and YP, YSC, and BKL contributed to supervision and funding acquisition. All authors have read and agreed to the published version of the manuscript.

Declarations

Conflict of interest The authors declare that they have no conflict of interest.

Ethical approval IACUC approve numbers: 2017-12-002 and 2017-12-068. All institutional and national guidelines for the care and use of laboratory animals were followed.

References

1. Kwong FNK, Harris MB (2008) Recent developments in the biology of fracture repair. J Am Acad Orthop Surg 16(11):619–625. https://doi.org/10.5435/00124635-200811000-00001
2. Roberts TT, Rosenbaum AJ (2012) Bone grafts, bone substitutes and orthobiologics: the bridge between basic science and clinical advancements in fracture healing. Organogenesis 8(4):114–124. https://doi.org/10.4161/org.23306
3. Albrektsson T, Johansson C (2001) Osteoinduction, osteoconduction and osseointegration. Eur Spine J 10(Suppl 2):S96–S101. https://doi.org/10.1007/s005860100282
4. Ben-Nissan B (2003) Natural bioceramics: from coral to bone and beyond. Curr Opin Solid State Mater Sci 7(4–5):283–288. https://doi.org/10.1016/j.cossms.2003.10.001
5. Fernandez JM, Molinuevo MS, Cortizo MS et al (2011) Development of an osteoconductive PCL–PDIPF–hydroxyapatite composite scaffold for bone tissue engineering. J Tissue Eng Regen Med 5(6):e126–e135. https://doi.org/10.1002/term.394
6. Nazirkar G, Singh S, Dole V et al (2014) Effortless effort in bone regeneration: a review. J Int Oral Health 6(3):120
7. Bae JC, Lee JJ, Shim JH et al (2017) Development and assessment of a 3D-printed scaffold with rhBMP-2 for an implant surgical guide stent and bone graft material: a pilot animal study. Materials 10(12):1434. https://doi.org/10.3390/ma10121434
8. Gautschi OP, Frey SP, Zellweger R (2007) Bone morphogenetic proteins in clinical applications. ANZ J Surg 77(8):626–631. https://doi.org/10.1111/j.1445-2197.2007.04175.x
9. Wei Y, Zhu G, Zhao Z et al (2021) Individualized plasticity autograft mimic with efficient bioactivity inducing osteogenesis. Int J Oral Sci 13(1):1–8. https://doi.org/10.1038/s41368-021-00120-w
10. James AW, LaChaud G, Shen J et al (2016) A review of the clinical side effects of bone morphogenetic protein-2. Tissue Eng Part B Rev 22(4):284–297. https://doi.org/10.1089/ten.TEB.2015.0357
11. McKay WF, Peckham SM, Badura JM (2007) A comprehensive clinical review of recombinant human bone morphogenetic protein-2 (INFUSE® Bone Graft). Int Orthop 31(6):729–734. https://doi.org/10.1007/s00264-007-0418-6
12. van Hout WM, van der Molen ABM, Breugem CC et al (2011) Reconstruction of the alveolar cleft: can growth factor-aided tissue engineering replace autologous bone grafting? A literature review and systematic review of results obtained with bone morphogenetic protein-2. Clin Oral Invest 15(3):297–303. https://doi.org/10.1007/s00784-011-0547-6

13. Li RH, Wozney JM (2001) Delivering on the promise of bone morphogenetic proteins. Trends Biotechnol 19(7):255–265. https://doi.org/10.1016/s0167-7799(01)01665-1
14. Mumcuoglu D, Fahmy-Garcia S, Ridwan Y et al (2018) Injectable BMP-2 delivery system based on collagen-derived microspheres and alginate induced bone formation in a time- and dose-dependent manner. Eur Cells Mater 35:242–254. https://doi.org/10.22203/eCM.v035a17
15. Kempen DH, Lu L, Hefferan TE et al (2008) Retention of in vitro and in vivo BMP-2 bioactivities in sustained delivery vehicles for bone tissue engineering. Biomaterials 29(22):3245–3252. https://doi.org/10.1016/j.biomaterials.2008.04.031
16. Lee JW, Kang KS, Lee SH et al (2011) Bone regeneration using a microstereolithography-produced customized poly (propylene fumarate)/diethyl fumarate photopolymer 3D scaffold incorporating BMP-2 loaded PLGA microspheres. Biomaterials 32(3):744–752. https://doi.org/10.1016/j.biomaterials.2010.09.035
17. Lee SJ, Lee D, Yoon TR et al (2016) Surface modification of 3D-printed porous scaffolds via mussel-inspired polydopamine and effective immobilization of rhBMP-2 to promote osteogenic differentiation for bone tissue engineering. Acta Biomater 40:182–191. https://doi.org/10.1016/j.actbio.2016.02.006
18. Park JY, Gao G, Jang J et al (2016) 3D printed structures for delivery of biomolecules and cells: tissue repair and regeneration. J Mater Chem B 4(47):7521–7539. https://doi.org/10.1039/c6tb01662f
19. Jang CH, Kim MS, Cho YB et al (2013) Mastoid obliteration using 3D PCL scaffold in combination with alginate and rhBMP-2. Int J Biol Macromol 62:614–622. https://doi.org/10.1016/j.ijbiomac.2013.10.011
20. Kang SW, Kim JS, Park KS et al (2011) Surface modification with fibrin/hyaluronic acid hydrogel on solid-free form-based scaffolds followed by BMP-2 loading to enhance bone regeneration. Bone 48(2):298–306. https://doi.org/10.1016/j.bone.2010.09.029
21. Park JY, Shim JH, Choi SA et al (2015) 3D printing technology to control BMP-2 and VEGF delivery spatially and temporally to promote large-volume bone regeneration. J Mater Chem B 3(27):5415–5425. https://doi.org/10.1039/c5tb00637f
22. Deng CJ, Lin RC, Zhang M et al (2019) Micro/nanometer-structured scaffolds for regeneration of both cartilage and subchondral bone. Adv Funct Mater 29(4):1806068. https://doi.org/10.1002/adfm.201806068
23. Zhang B, Gui X, Song P et al (2022) Three-dimensional printing of large-scale, high-resolution bioceramics with micronano inner porosity and customized surface characterization design for bone regeneration. ACS Appl Mater Interf 14(7):8804–8815. https://doi.org/10.1021/acsami.1c22868
24. Zhang B, Wang W, Gui X et al (2022) 3D printing of customized key biomaterials genomics for bone regeneration. Appl Mater Today 26:101346. https://doi.org/10.1016/j.apmt.2021.101346
25. Pei X, Wu L, Lei H et al (2021) Fabrication of customized Ti6AI4V heterogeneous scaffolds with selective laser melting: optimization of the architecture for orthopedic implant applications. Acta Biomater 126:485–495. https://doi.org/10.1016/j.actbio.2021.03.040
26. Lee SH, Cho YS, Hong MW et al (2017) Mechanical properties and cell-culture characteristics of a polycaprolactone kagome-structure scaffold fabricated by a precision extruding deposition system. Biomed Mater 12(5):055003. https://doi.org/10.1088/1748-605X/aa8357
27. Lee SH, Lee KG, Hwang JH et al (2019) Evaluation of mechanical strength and bone regeneration ability of 3D printed kagome-structure scaffold using rabbit calvarial defect model. Mater Sci Eng C 98:949–959. https://doi.org/10.1016/j.msec.2019.01.050
28. Cho YS, Quan M, Kang NU et al (2020) Strategy for enhancing mechanical properties and bone regeneration of 3D polycaprolactone kagome scaffold: nano hydroxyapatite composite and its exposure. Eur Polymer J 134:109814. https://doi.org/10.1016/j.eurpolymj.2020.109814
29. Wang AJ, McDowell D (2004) In-plane stiffness and yield strength of periodic metal honeycombs. J Eng Mater Technol 126(2):137–156. https://doi.org/10.1115/1.1646165
30. Yun BG, Lee SH, Jeon JH et al (2019) Accelerated bone regeneration via three-dimensional cell-printed constructs containing human nasal turbinate-derived stem cells as a clinically applicable therapy. ACS Biomater Sci Eng 5(11):6171–6185. https://doi.org/10.1021/acsbiomaterials.9b01356
31. Kim BS, Jang J, Chae S et al (2016) Three-dimensional bioprinting of cell-laden constructs with polycaprolactone protective layers for using various thermoplastic polymers. Biofabrication 8(3):035013. https://doi.org/10.1088/1758-5090/8/3/035013
32. Kim J, Park Y, Tae G et al (2008) Synthesis and characterization of matrix metalloprotease sensitive-low molecular weight hyaluronic acid based hydrogels. J Mater Sci Mater Med 19(11):3311–3318. https://doi.org/10.1007/s10856-008-3469-3
33. Ku JK, Lee KG, Ghim MS et al (2021) Onlay-graft of 3D printed kagome-structure PCL scaffold incorporated with rhBMP-2 based on hyaluronic acid hydrogel. Biomed Mater 16(5):055004. https://doi.org/10.1088/1748-605X/ac0f47
34. Kim J, Kim IS, Cho TH et al (2007) Bone regeneration using hyaluronic acid-based hydrogel with bone morphogenic protein-2 and human mesenchymal stem cells. Biomaterials 28(10):1830–1837. https://doi.org/10.1016/j.biomaterials.2006.11.050
35. Reyes RL, Ghim MS, Kang NU et al (2022) Development and assessment of modified-honeycomb-structure scaffold for bone tissue engineering. Addit Manuf 54:102740. https://doi.org/10.1016/j.addma.2022.102740
36. Patterson J, Siew R, Herring SW et al (2010) Hyaluronic acid hydrogels with controlled degradation properties for oriented bone regeneration. Biomaterials 31(26):6772–6781. https://doi.org/10.1016/j.biomaterials.2010.05.047
37. Kim J, Park Y, Tae G et al (2009) Characterization of low-molecular-weight hyaluronic acid-based hydrogel and differential stem cell responses in the hydrogel microenvironments. J Biomed Mater Res A 88(4):967–975. https://doi.org/10.1002/jbm.a.31947
38. Lutolf MP, Lauer-Fields JL, Schmoekel HG et al (2003) Synthetic matrix metalloproteinase-sensitive hydrogels for the conduction of tissue regeneration: engineering cell-invasion characteristics. Proc Natl Acad Sci 100(9):5413–5418. https://doi.org/10.1073/pnas.0737381100
39. Schultz KM, Kyburz KA, Anseth KS (2015) Measuring dynamic cell–material interactions and remodeling during 3D human mesenchymal stem cell migration in hydrogels. Proc Natl Acad Sci 112(29):E3757–E3764. https://doi.org/10.1073/pnas.1511304112
40. Kim J, Kim IS, Cho TH et al (2010) In vivo evaluation of MMP sensitive high-molecular weight HA-based hydrogels for bone tissue engineering. J Biomed Mater Res Part A 95(3):673–681. https://doi.org/10.1002/jbm.a.32884
41. Mumcuoglu D, Siverino C, Tabisz B et al (2017) How to use BMP-2 for clinical applications? A review on pros and cons of existing delivery strategies. J Trans Sci 3(5):1–11. https://doi.org/10.15761/JTS.1000195
42. Li J, Mooney DJ (2016) Designing hydrogels for controlled drug delivery. Nat Rev Mater 1(12):1–17. https://doi.org/10.1038/natrevmats.2016.71
43. Shim JH, Kim JY, Park M et al (2011) Development of a hybrid scaffold with synthetic biomaterials and hydrogel using solid freeform fabrication technology. Biofabrication 3(3):034102. https://doi.org/10.1088/1758-5082/3/3/034102
44. Shim JH, Lee JS, Kim JY et al (2012) Bioprinting of a mechanically enhanced three-dimensional dual cell-laden construct for osteochondral tissue engineering using a multi-head tissue/organ

building system. J Micromech Microeng 22(8):085014. https://doi.org/10.1088/0960-1317/22/8/085014
45. Lee F, Chung JE, Kurisawa M (2009) An injectable hyaluronic acid–tyramine hydrogel system for protein delivery. J Contr Release 134(3):186–193. https://doi.org/10.1016/j.jconrel.2008.11.028
46. Bhakta G, Rai B, Lim ZX et al (2012) Hyaluronic acid-based hydrogels functionalized with heparin that support controlled release of bioactive BMP-2. Biomaterials 33(26):6113–6122. https://doi.org/10.1016/j.biomaterials.2012.05.030
47. Ishidou Y, Kitajima I, Obama H et al (1995) Enhanced expression of type I receptors for bone morphogenetic proteins during bone formation. J Bone Mine Res 10(11):1651–1659. https://doi.org/10.1002/jbmr.5650101107
48. Spector JA, Luchs JS, Mehrara BJ et al (2001) Expression of bone morphogenetic proteins during membranous bone healing. Plastic Reconstruct Surg 107(1):124–134. https://doi.org/10.1097/00006534-200101000-00018
49. La WG, Kang SW, Yang HS et al (2010) The efficacy of bone morphogenetic protein-2 depends on its mode of delivery. Artif Organs 34(12):1150–1153. https://doi.org/10.1111/j.1525-1594.2009.00988.x
50. Yang HS, La WG, Cho YM et al (2012) Comparison between heparin-conjugated fibrin and collagen sponge as bone morphogenetic protein-2 carriers for bone regeneration. Exp Mol Med 44(5):350–355. https://doi.org/10.3858/emm.2012.44.5.039
51. Uludag H, Golden J, Palmer R et al (1999) Biotinated bone morphogenetic protein-2: in vivo and in vitro activity. Biotechnol Bioeng 65(6):668–672. https://doi.org/10.1002/(sici)1097-0290(19991220)65:6%3c668::aid-bit7%3e3.0.co;2-8
52. Haidar ZS, Hamdy RC, Tabrizian M et al (2009) Delivery of recombinant bone morphogenetic proteins for bone regeneration and repair. Part A: current challenges in BMP delivery. Biotechnol Lett 31(12):1817–1824. https://doi.org/10.1007/s10529-009-0099-x